Electronic Supporting Information

# Impact of the hybridization form for coordination nitrogen atom on the electrocatalytic water oxidation performance of copper complexes with pentadentate amine-pyridine ligands

Kaishan Yu‡[a,b], Tao Wang,‡[a] Yue Sun,[a] Mei Kang,[a] Xinxin Wang,[a] Dingwei Zhu,[a] Siyi Xue,[a] Junyu Shen,*[a] Qijian Zhang,*[a] and Jinxuan Liu*[b]

[a] *Jiangsu Laboratory of Advanced Functional Materials, School of Materials Engineering, Changshu Institute of Technology, Changshu 215500, P. R. China.*

[b] *State Key Laboratory of Fine Chemicals, Dalian University of Technology (DUT), Dalian 116024, P. R. China.*

‡ *These authors contributed equally to this work.*

* *Corresponding author, E-mail: shenjunyu2014@126.com (Junyu Shen)*
*flashright@163.com (Qijian Zhang)*
*jinxuan.liu@dlut.edu.cn (Jinxuan Liu)*

**Instruments:** NMR Spectra were collected with a Varian INOVA 500 NMR spectrometer. Mass spectra were recorded with HP 1100 HPL/ESI-DAD-MS and Waters/Micromass LC/Q-TOF-MS instruments. Elemental analyses were performed with a Thermoquest-Flash EA 1112 elemental analyzer. UV-Vis absorption measurements were carried out on an Agilent 8453 spectrophotometer. SEM images and EDX spectra were obtained with a HITACHI UHR FE-SEM SU8220 instrument equipped with an EDX detector. XPS surveys were acquired with a Thermo Fisher ESCALAB 250Xi surface analysis system. The measurements of dynamic light scattering (DLS) spectra were measured with a Zetasizer Nano ZS90 instrument. EPR

spectra were collected on a Bruker EPR spectrometer (A200) with microwave frequency of 9.86 GHz at room temperature.

**Crystallographic structure determinations.** The single-crystal X-ray diffraction data were collected on a Bruker Smart Apex II CCD diffractometer with a graphite-monochromated Mo-$K_\alpha$ radiation ($\lambda$ = 0.071073 Å) at 296 K using the $\omega$-2$\theta$ scan mode. Data processing was accomplished with the SAINT processing program.[S3] Intensity data were corrected for absorption by the SADABS program.[S4] All structures were solved by direct methods and refined on $F^2$ against full-matrix least-squares methods by using the SHELXTL 97 program package.[S5] Non-hydrogen atoms were refined anisotropically. Hydrogen atoms were located by geometrical calculation. Crystallographic data and selected bond lengths and angles for **1** and **2** are given in Tables S1 and S2 (CCDC number: 2305144 for **1** and 2020089 for **2**).

**CV experiments.** Cyclic voltammetry experiments were carried out in a three-electrode cell under argon. The working electrode was a glassy carbon electrode disc (0.071 $cm^2$), the reference electrode was an aqueous Ag/AgCl electrode, and the counter electrode was a platinum wire. The solution of 0.1 M phosphate buffer at pH 11.0 was used as supporting electrolyte, which was degassed by bubbling with argon for 15 min before measurement. All potentials are reported versus the normal hydrogen electrode (NHE) by addition of 0.197 V to the experimentally measured values.

**CPE experiments**. The controlled potential electrolysis (CPE) experiment was carried out in a home-made H-type electrochemical cell with an FTO (1.0 $cm^2$) glass slide as working electrode. The auxiliary electrode was a platinum wire which was protected by a casing pipe and the reference electrode was a commercially available aqueous Ag/AgCl electrode. The sample was bubbled with argon for 20 min before measurement with constantly stirring.

**The determination of FE**. The Faradaic efficiency (FE) was determined from CPE experiments of the solutions of **1** and **2** in 0.1 M phosphate buffer at pH 11.0 in a custom-built gas-tight electrochemical cell at an applied potential of 1.6 V vs NHE for 3 h. The gas in the headspace of the cell was analyzed by CEAULIGHT GC-7920 gas chromatograph equipped with a 5 Å molecular sieve column (2 mm × 2 m) during the electrolysis and the oxygen dissolved in the solution was neglected. Faradaic efficiencies of electrochemical $O_2$ evolution were determined according to the amount of $O_2$ evolved and the amount of $O_2$ calculated from the total consumed charge during the CPE experiment by assuming a $4e^-$ catalytic process (eq. 1).

$$\mathrm{FE} = \frac{\text{Produced } O_2\ (n_{measured})}{\text{Calculated } O_2\ (n_{calculated})} \times 100\% \qquad \text{(eq.1)}$$

Produced oxygen was obtained from peak area of gas chromatograph and standard curve of $O_2$. Calculated oxygen can be got through the eq. 2:

$$n_{calculated} = \frac{Q}{n \times e \times NA} \qquad \text{(eq.2)}$$

Where $Q$ is the total amount of charge consumed during electrolysis, $n$ is number

of electron transferred for water oxidation ($n$ = 4), $e$ is the elementary charge ($e$ = 1.6 $\times$ $10^{-19}$ C), $NA$ is Avogadro constant ($NA$ = 6.02 $\times$ $10^{23}$).

**Kinetic equations.**

$$i_d = 0.4463 n_d F A [Cu](n_d F v D_{Cu}/RT)^{1/2} \qquad \text{(eq. 3)}$$

$$i_c = n_c F A [Cu](k_{cat} D_{Cu})^{1/2} \qquad \text{(eq. 4)}$$

$$i_c/i_d = 2.24 n_c n_d^{3/2}(k_{cat} RT)^{1/2}(Fv)^{-1/2} \qquad \text{(eq. 5)}$$

where $i_d$ is the plateau current density of noncatalytic wave (here taken from the peak current of $Cu^{I}$ to $Cu^{II}$), $n_d$ is the number of electron transferred for the $Cu^{II}/Cu^{I}$ couple ($n_d$ = 1), $v$ is the scan rate, $R$ is the universal gas constant, and $T$ is the temperature in Kelvin ($T$ = 298.15 K), $i_c$ is the limiting catalytic peak current, $n_c$ is the number of electrons transferred for producing a molecule of $O_2$ in water oxidation ($n_c$ = 4), $F$ is Faraday constant, $A$ is the surface area of the electrode (in $cm^2$), [Cu] is the initial concentration of catalyst (in mol $L^{-1}$), $k_{cat}$ is the apparent first-order rate constant, and $D_{Cu}$ is the diffusion coefficient of the copper catalyst in 0.1 M phosphate buffer solution at pH 11.0.

Substituting data into eq. 5, it could be simplified to eq. 6.

$$i_c/i_d = 1.436(k_{cat}/v)^{1/2} \qquad \text{(eq. 6)}$$

**Testing peroxide intermediates formed during CPE experiments in electrolytes.** Ampliflu red (AR) was dissolved in DMSO and horseradish peroxidase (HRP) in 0.5 M PBS, both in a concentration of 0.4 mg $mL^{-1}$. The controlled potential electrolysis

(CPE) experiment of complex **1** (1 mM) in 0.1 M PBS at pH 11 was carried out at 1.6 V vs. NHE in an electrochemical cell. A fluorine-doped tin oxide (FTO) with a surface area of 1.5 $cm^2$ was used as working electrode. After 3 h of electrolysis, the HRP solution (1.0 mL) and AR solution (1.0 mL) were successively added into the resulting electrolyte (3.0 mL). The blue color of the solution turned pink after the sample was stirred for about 15 s (Fig. S16).

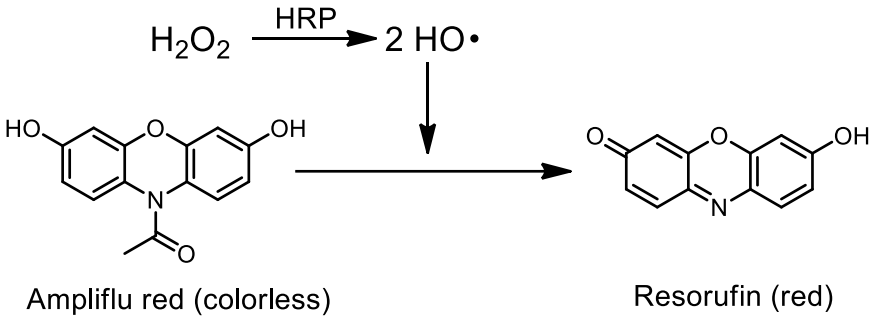


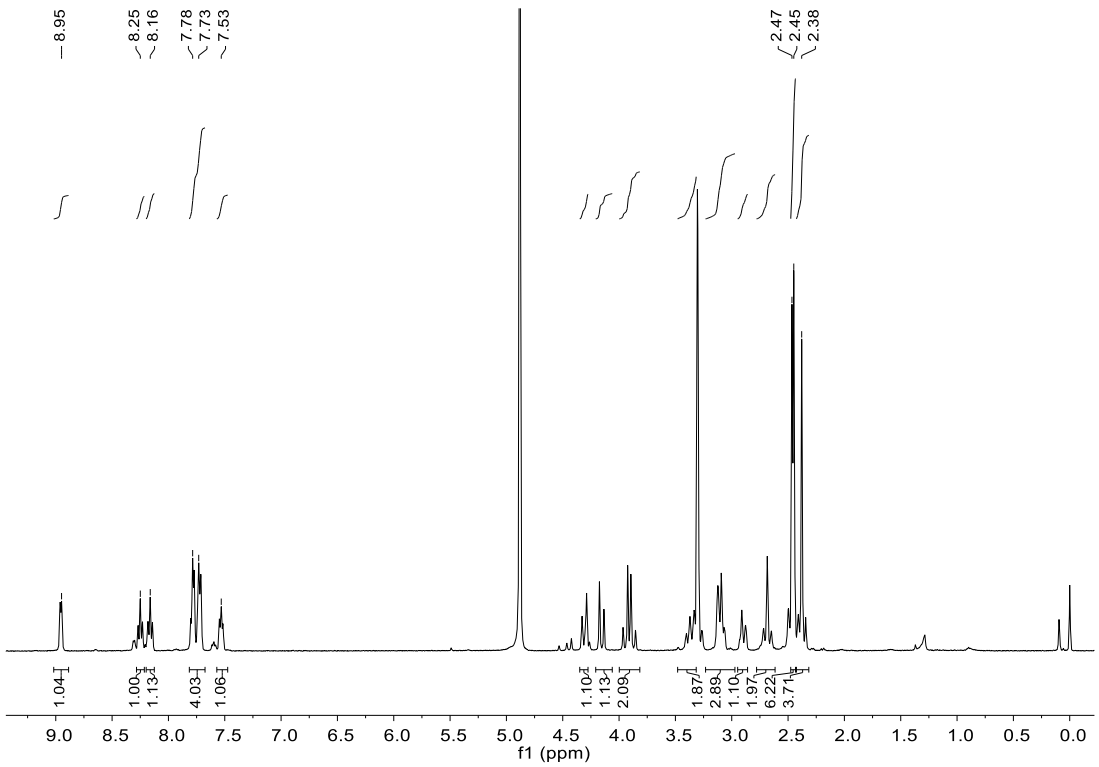


**Fig. S1** $^1$H-NMR of $[Zn(N_3Py_2)](BF_4)_2$

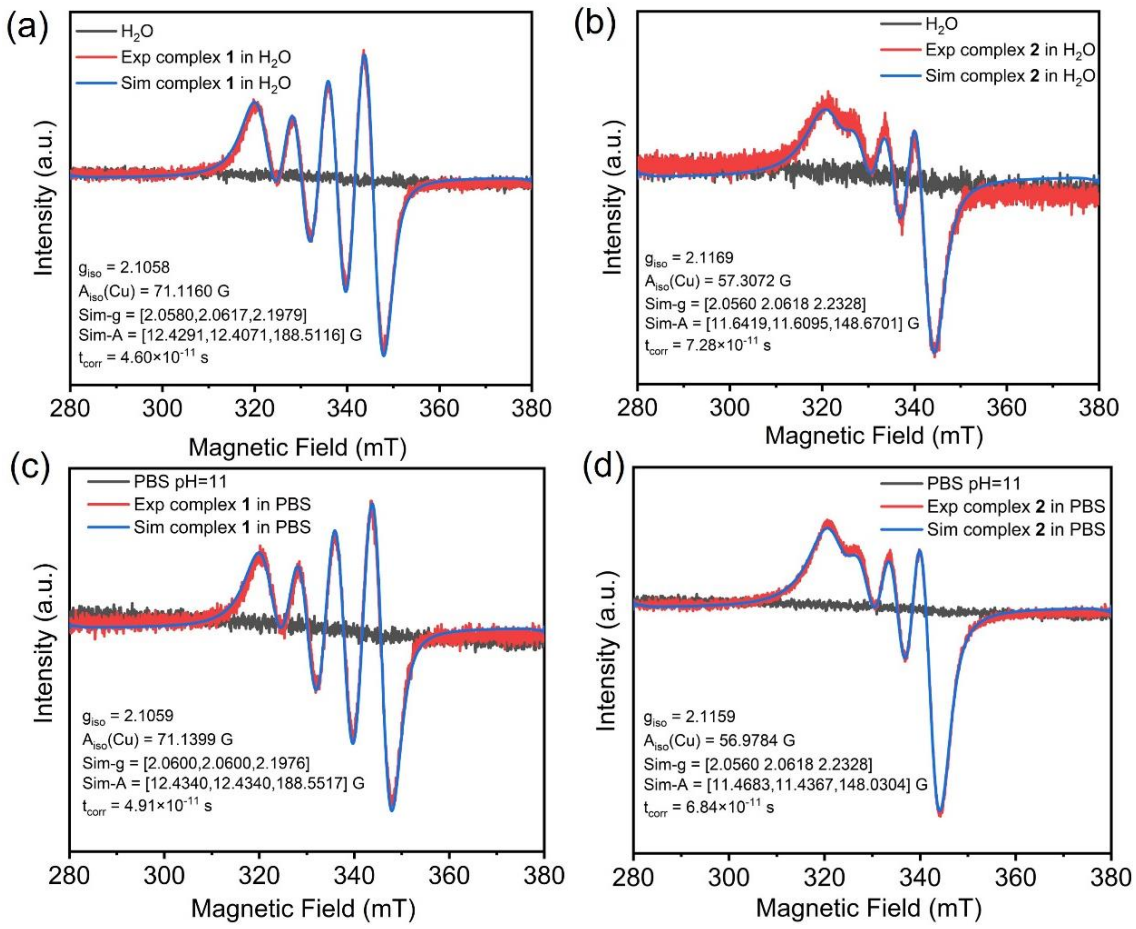


**Fig. S2** Continuous wave X-band EPR spectra of (a) (c) complex **1** and (b) (d) complex **2** (both in 10 mM) in $H_2O$ and in 0.1 M PBS at pH 11.

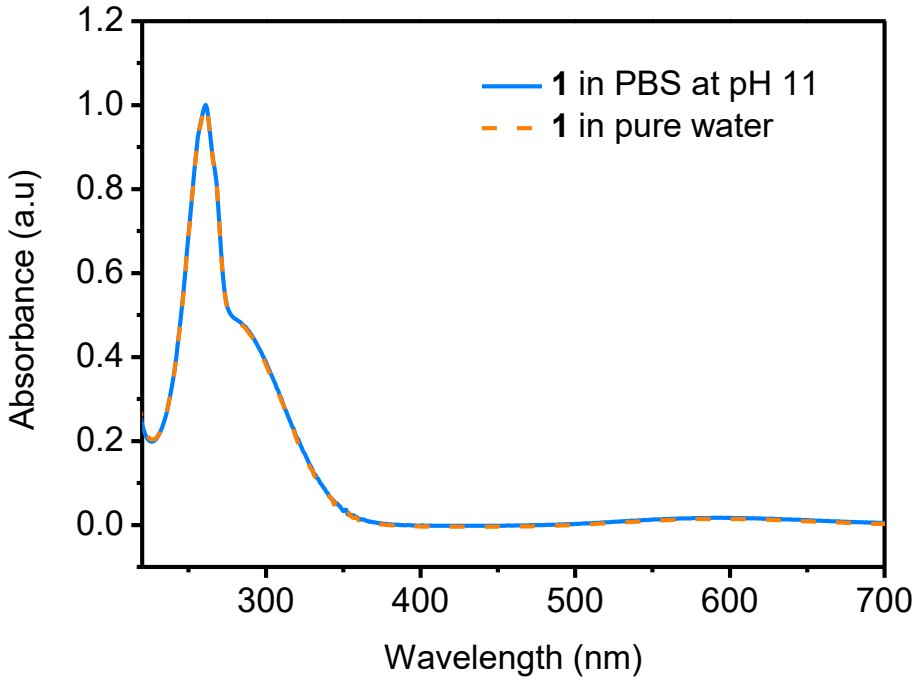


**Fig. S3** UV-vis spectra of **1** (0.1 mM) in 0.1 M PBS at pH 11 and pure water (optical length: 10 mm).

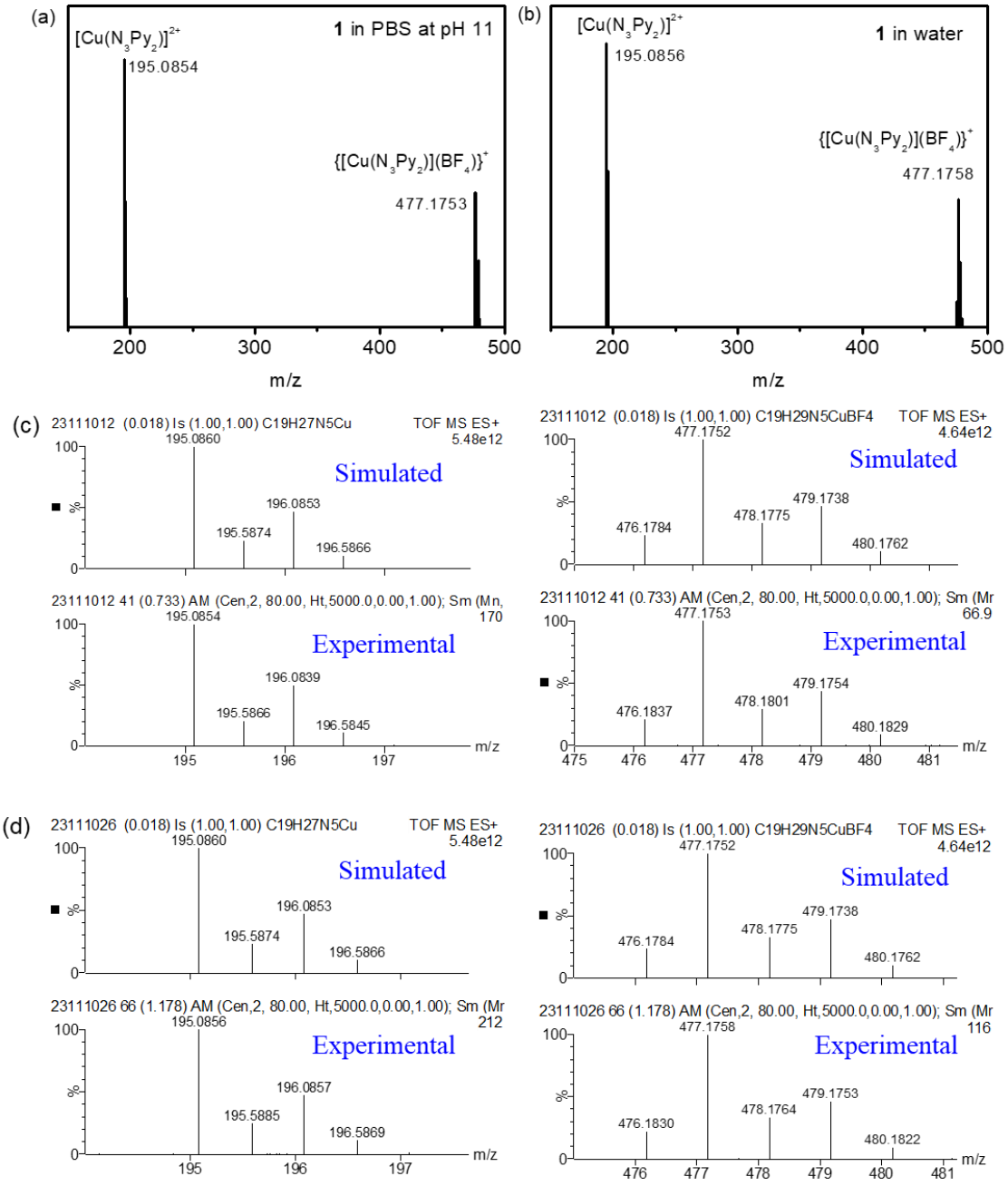


**Fig. S4** HRMS of **1** in (a) 0.1 M PBS at pH 11 and (b) pure water. The isotopic analysis of **1** in (c) 0.1 M PBS at pH 11 and (d) pure water.

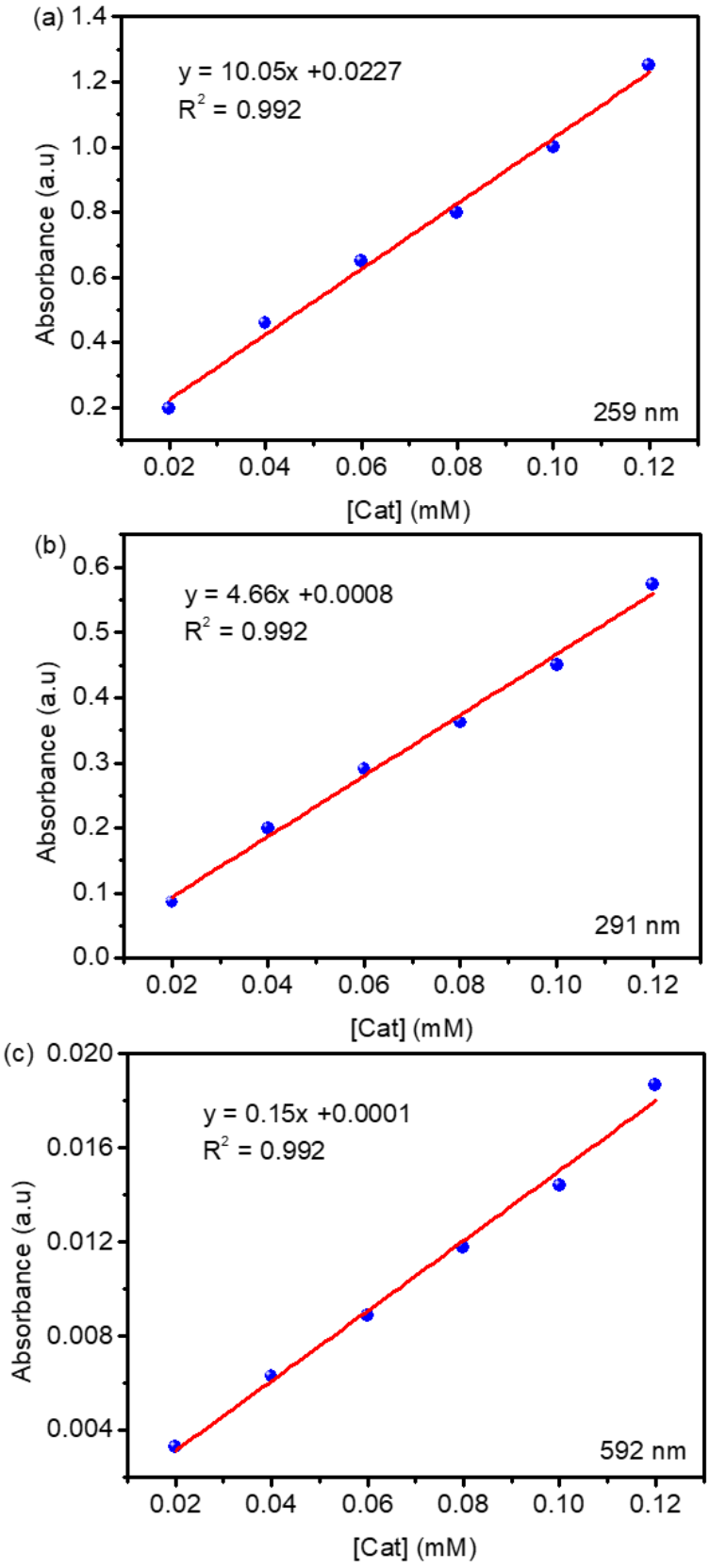


**Fig. S5** Plots of the absorbance intensity at (a) 259 nm, (b) 291 nm and (c) 592 nm versus the concentration of **1** (from 0.02 to 0.12 mM, optical length: 10 mm).

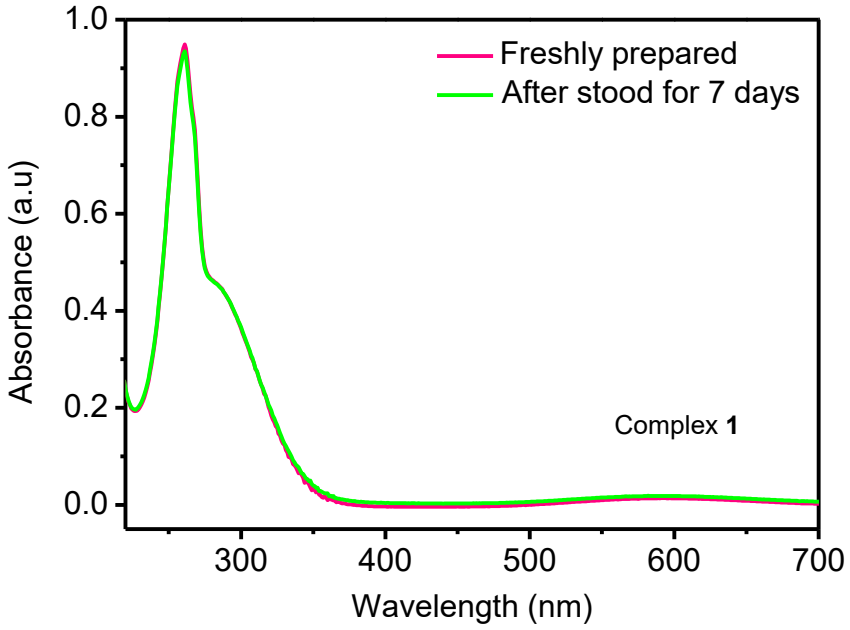


**Fig. S6** Comparison of UV-vis spectra of **1** (0.1 mM) in 0.1 M PBSs measured when freshly prepared and after stood for a week under air (optical length: 10 mm).

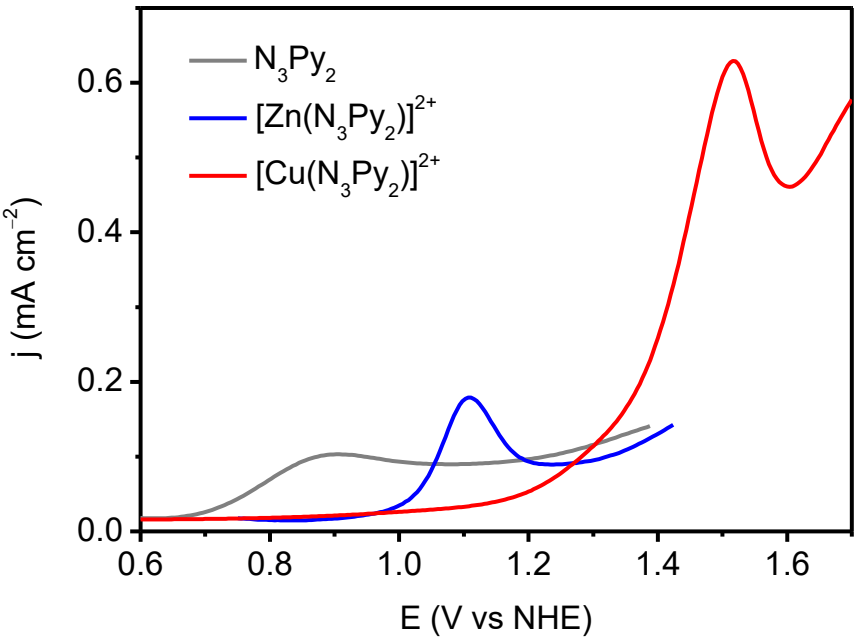


**Fig. S7** DPV curves of $N_3Py_2$, $[Zn(N_3Py_2)]^{2+}$ and **1** (all in 1.0 mM) and blank in 0.1 M PBSs at pH 11 at a scan rate of 8 mV $s^{-1}$.

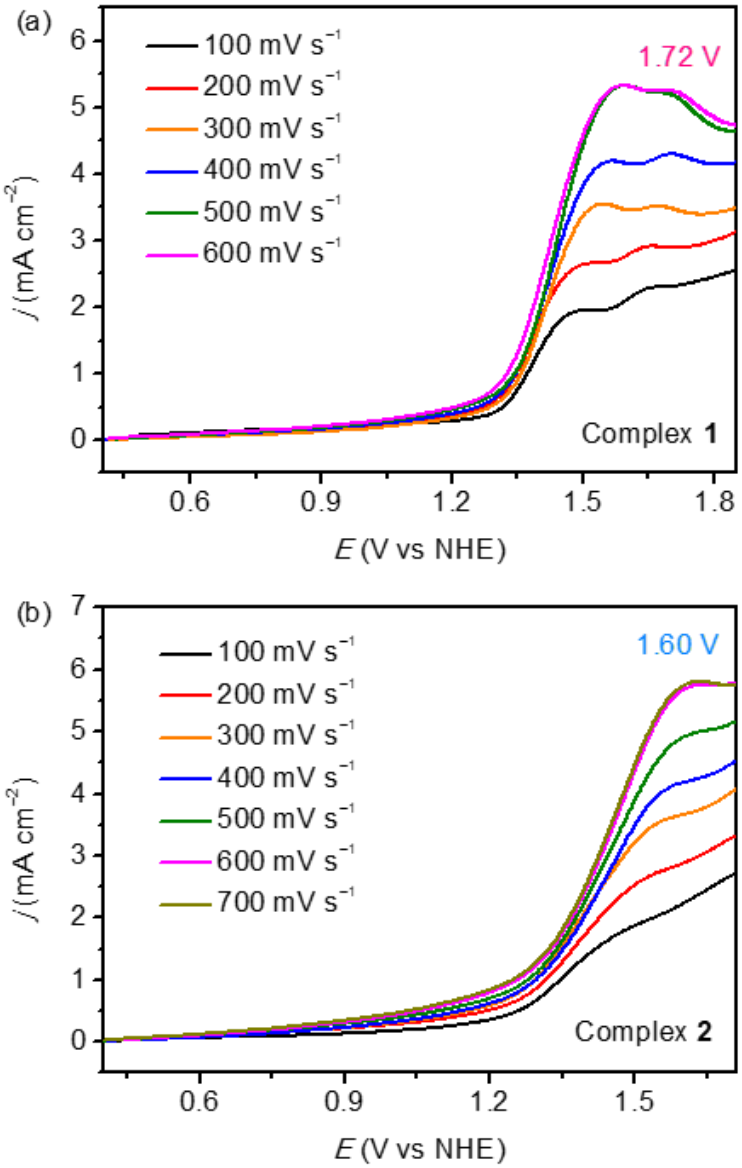


**Fig. S8** Linear voltammograms of (a) **1** and (b) **2** (both in 1.0 mM) in 0.1 M PBSs at pH 11 with scan rate varying from 100 to 700 mV $s^{-1}$.

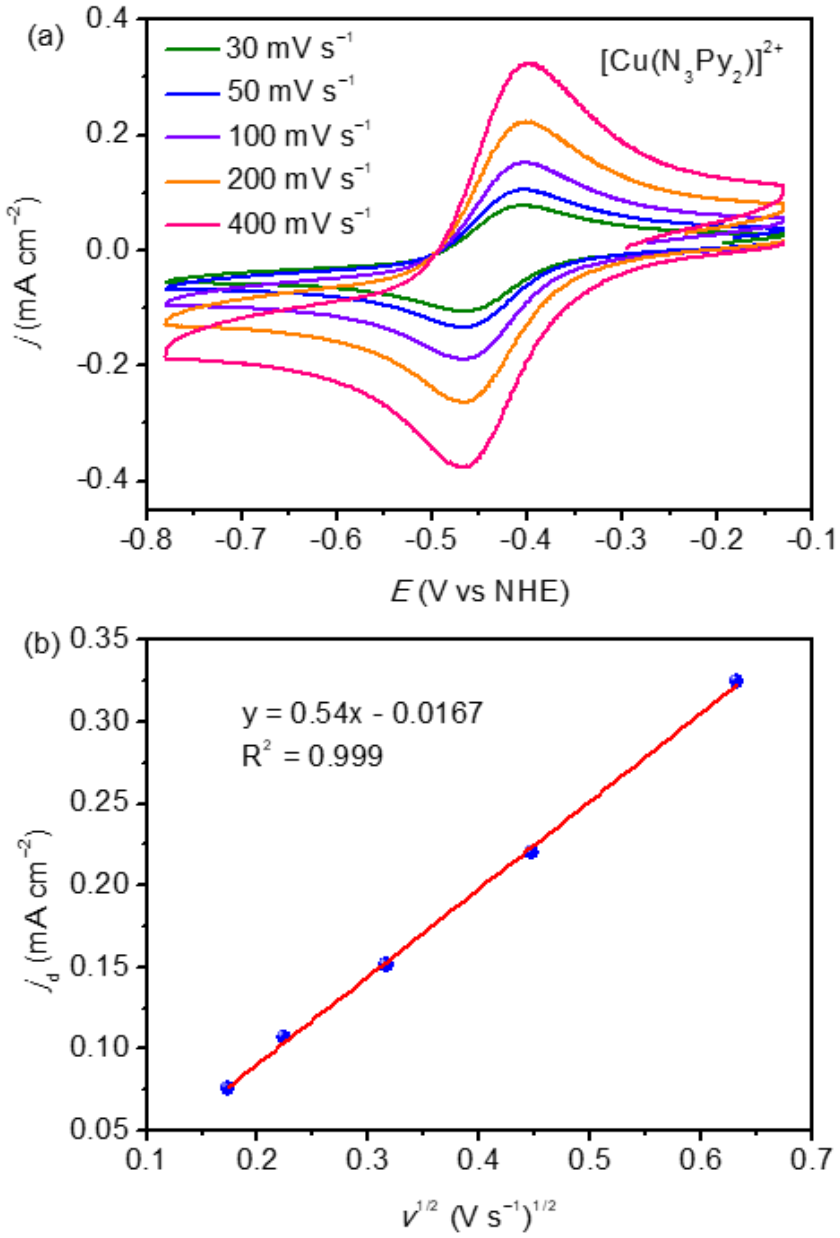


**Fig. S9** (a) Cyclic voltammograms of **1** (1.0 mM) in 0.1 M PBSs at pH 11 with scan rate varying from 30 to 400 mV $s^{-1}$. (b) Plot of the anodic current density maximum of the $Cu^{II}/Cu^{I}$ couple as a function of the square root of scan rate.

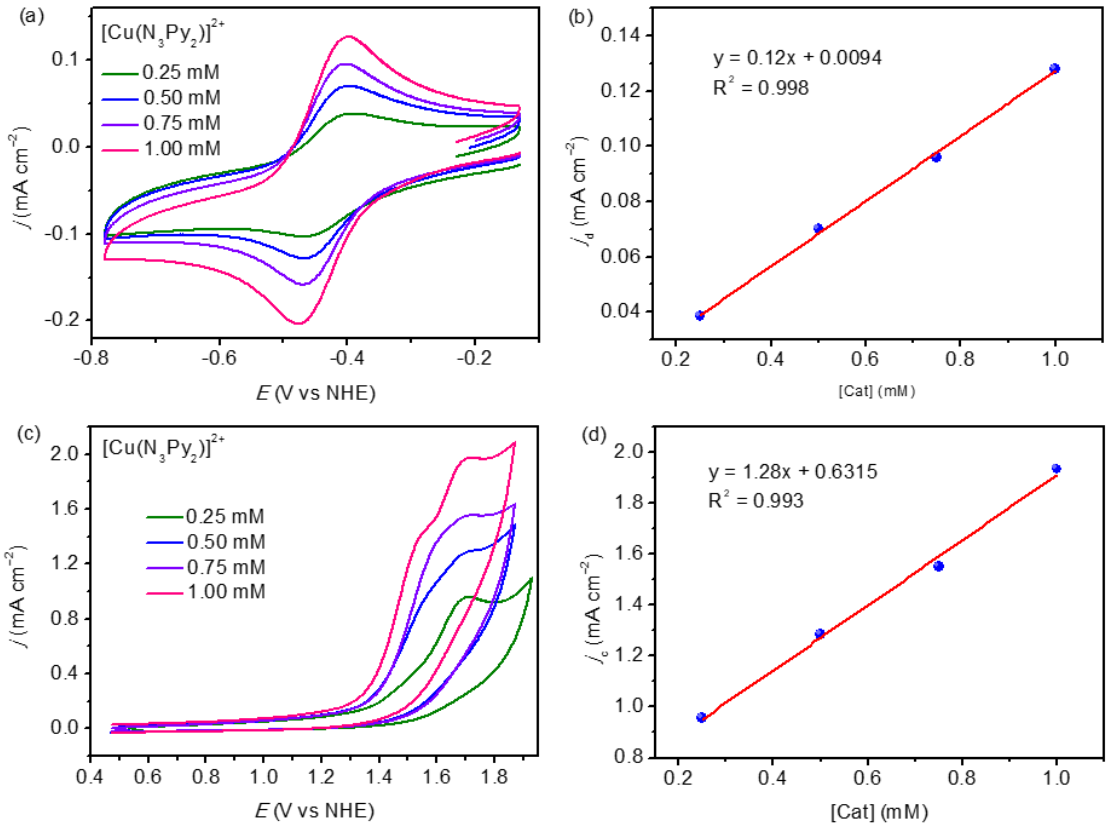


**Fig. S10** (a) Cyclic voltammograms of **1** in 0.1 M PBSs at pH 11 at a scan rate of 100 mV $s^{-1}$ with the concentration of **1** varying from 0.25 to 1.00 mM (scan range from –0.78 to –0.18 V). (b) Plots of the current density maxima ($j_d$), as a function of catalyst concentration. (c) Cyclic voltammograms of **1** in 0.1 M PBSs at pH 11 at a scan rate of 100 mV $s^{-1}$ with the concentration of **1** varying from 0.25 to 1.00 mM (scan range from 0.48 to 1.9 V). (d) Plots of the current density maxima ($j_c$), as a function of catalyst concentration.

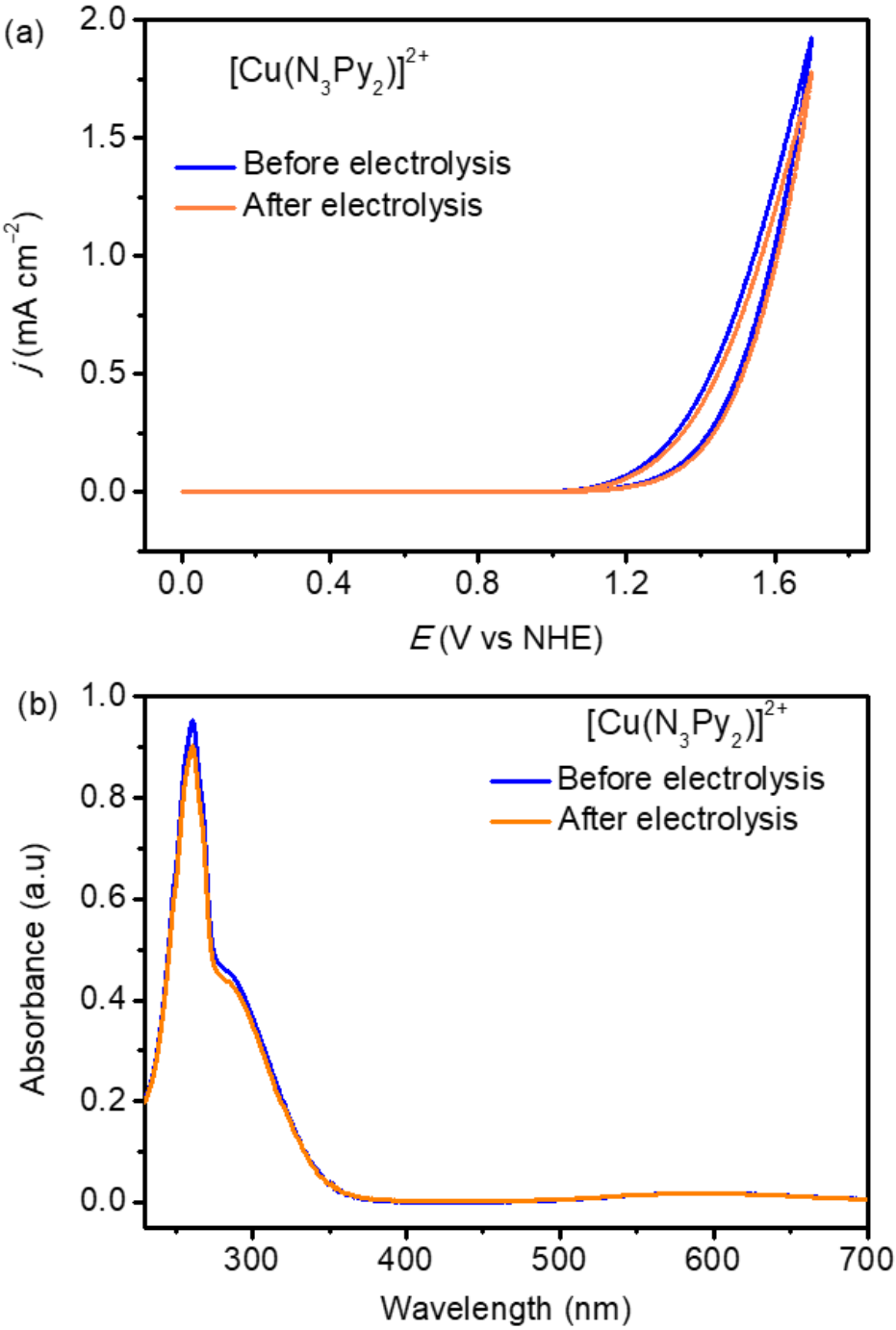


**Fig. S11** (a) CVs of **1** (1.0 mM) in 0.1 M PBSs at pH 11 at a scan rate of 100 mV $s^{-1}$ with an FTO electrode (1 $cm^2$) before and after electrolysis. (b) UV-vis spectra of **1** (both in 0.1 mM) in 0.1 M PBSs at pH 11 before and after electrolysis (optical length: 10 mm). Current density attenuation: 6.5%, concentration reduction: 6.0%.

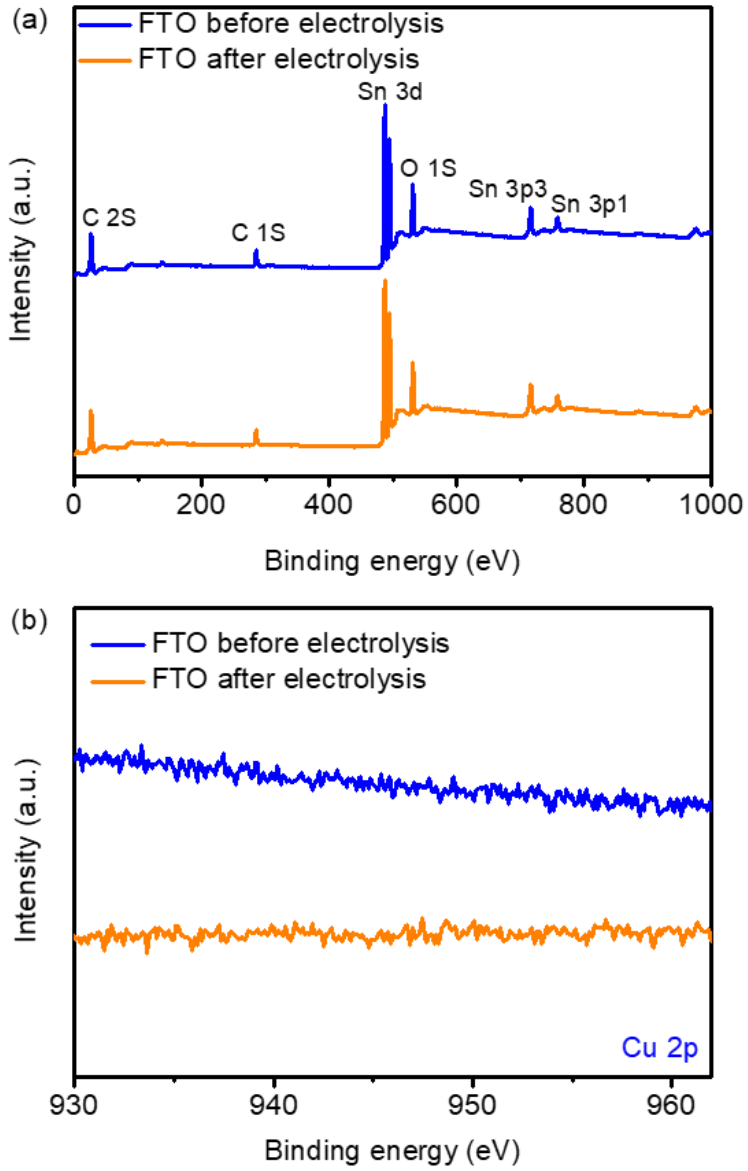


**Fig. S12** (a) XPS surveys of FTO before and after 3 h of CPE experiment with **1** as a catalyst. (b) XPS spectra of Cu 2p for FTO before and after 3 h electrolysis with **1** as a catalyst.

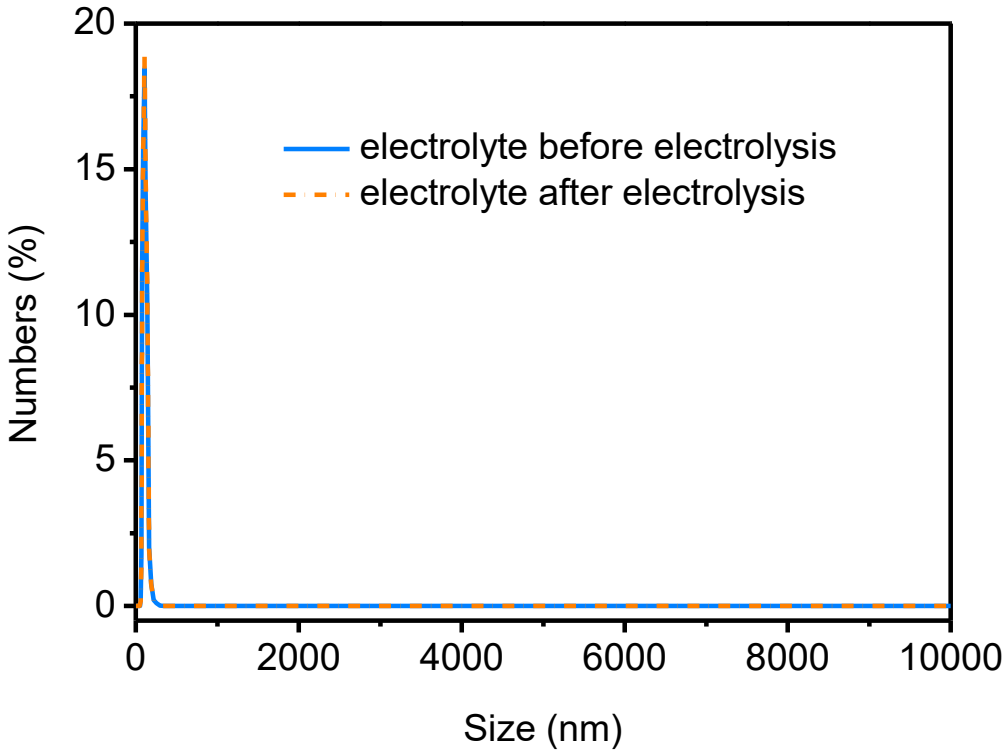


**Fig. S13** DLS spectra of electrolytes before and after 3 h of electrolysis with **1** as a catalyst. The electrolyte was filtered through hydrophilic filter membrane of 220 nm. Peaks between 100-200 nm are caused by dust in the air.

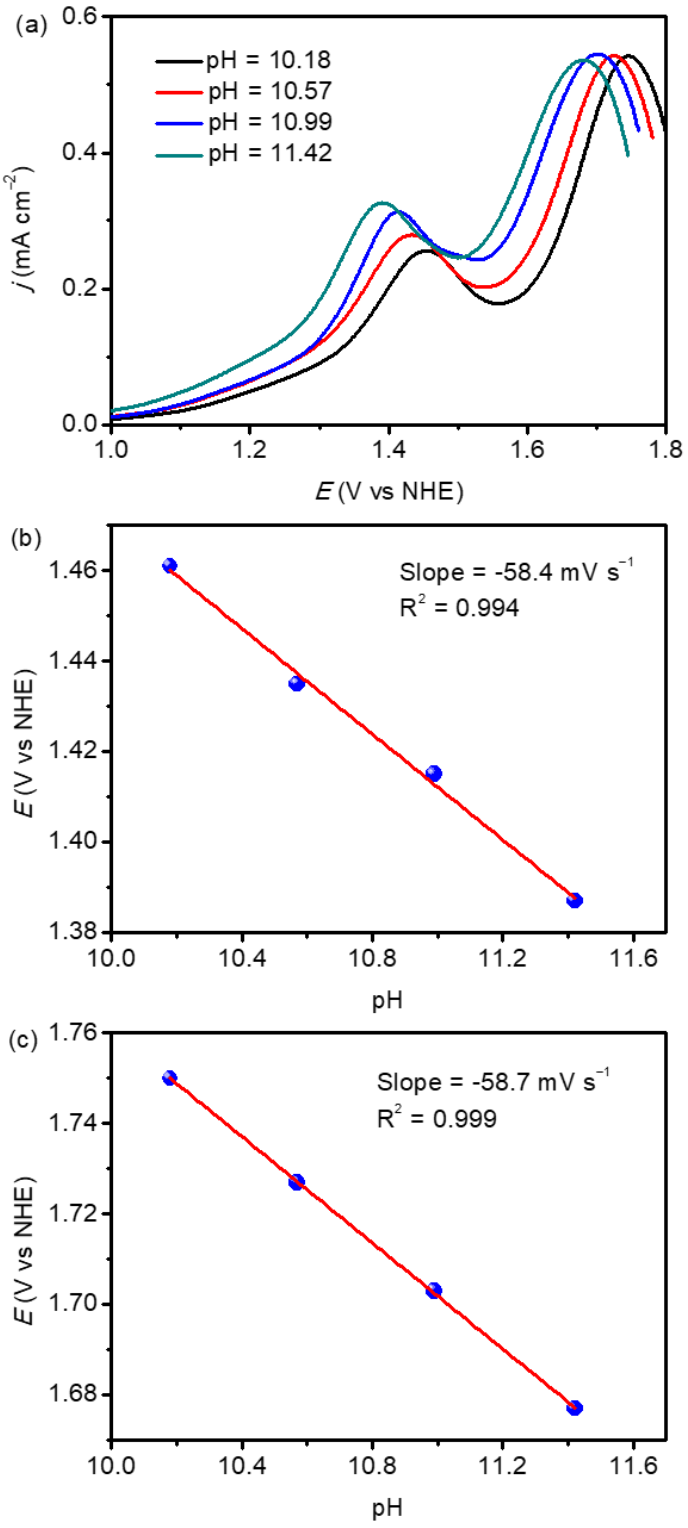


**Fig. S14** (a) DPV of **1** (1.0 mM) in 0.1 M PBSs with pH varied from 10.18 to 11.42 at a scan rate of 1 mV $s^{-1}$ (to better observe the peak potential, the background current density has been subtracted). Pourbaix plots of (b) the first and (c) the second oxidation peak for **1**.

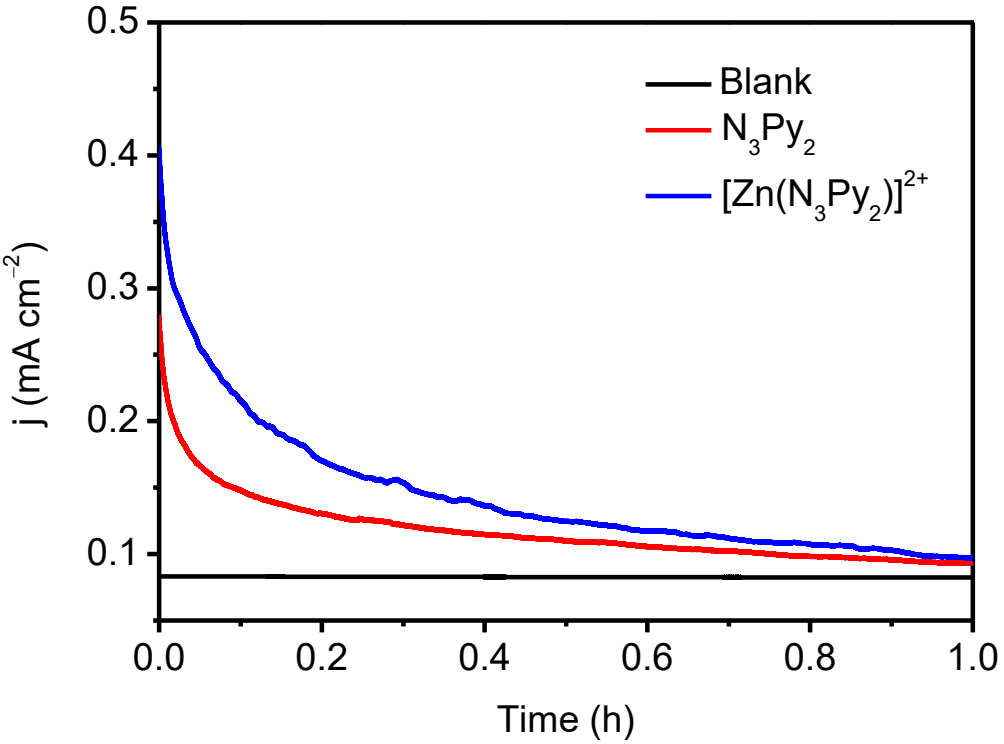


**Fig. S15** CPE experiments of $N_3Py_2$ and $[Zn(N_3Py_2)]^{2+}$ at 1.6 V vs. NHE in 0.1 M PBSs at pH 11.0

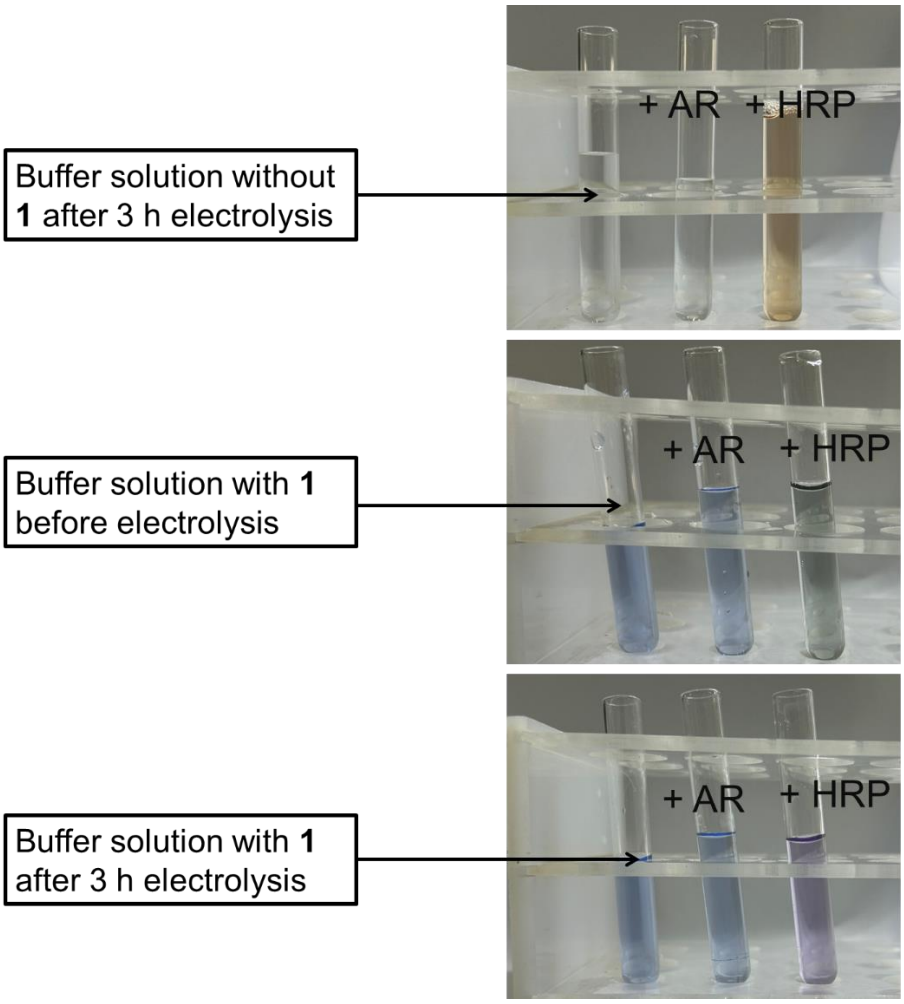


**Fig. S16** Experiments for testing the peroxide intermediates in the resulting electrolytes after 3 h of electrolysis of **1** in pH 11.0, 0.1 M PBSs, using horseradish peroxidase (HRP, a special catalyst for hemolysis of the peroxide bond of $H_2O_2$ to form $^{\bullet}OH$ radicals) and Ampliflu red (AR, a reliable titrant for $^{\bullet}OH$).

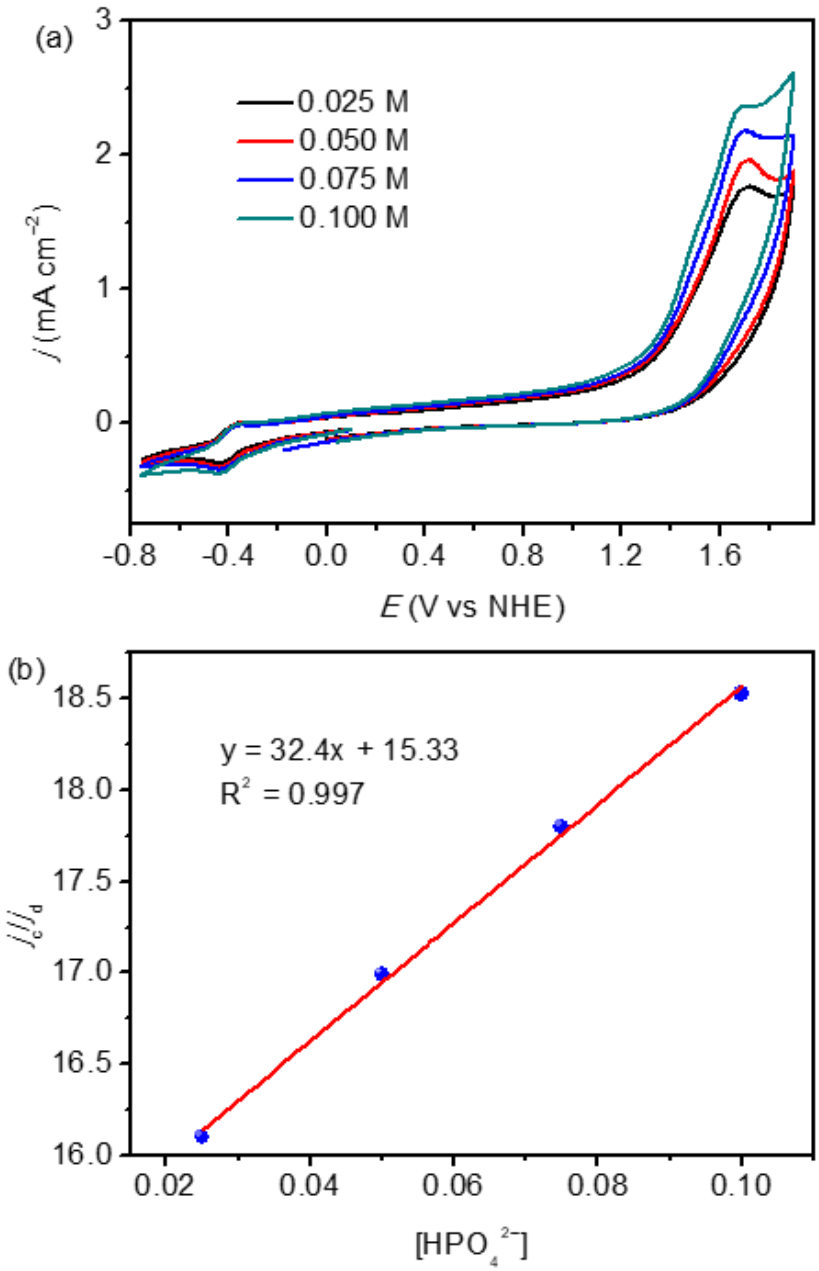


**Fig. S17** (a) Cyclic voltammograms of **1** at a scan rate of 100 mV $s^{-1}$ with the concentration of phosphate buffer solution varied from 0.025 to 0.1 M at pH 11. (b) Plots of $(j_c/j_d)^2$ as a function of $[HPO_4^{2-}]$ at constant concentration of **1**.

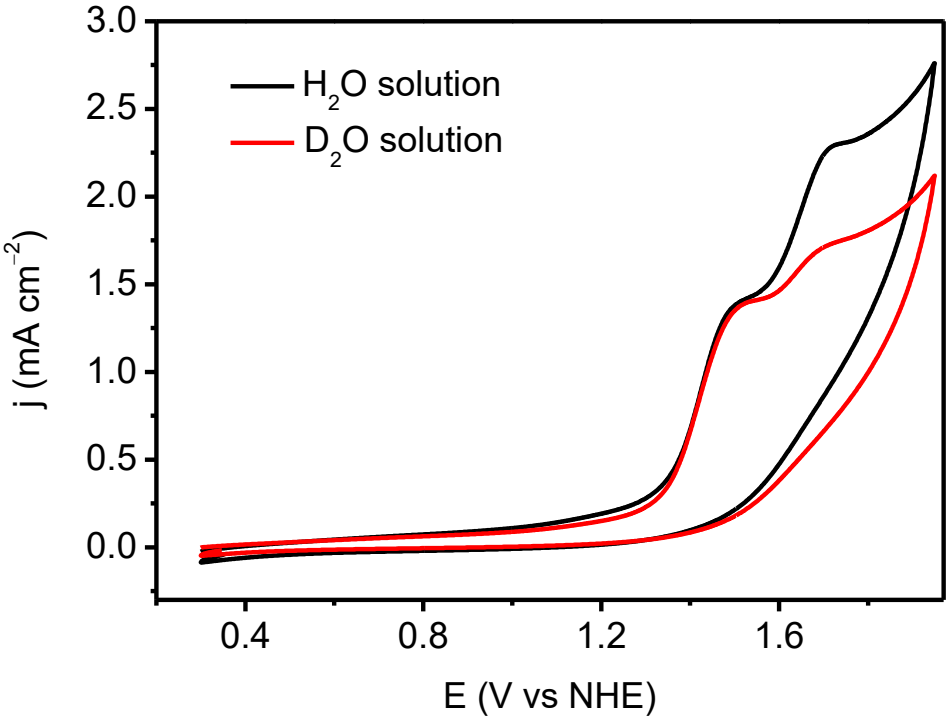


**Fig. S18** CV of **1** in $H_2O$ or $D_2O$ PBSs at pH 11 with glassy carbon as working electrode at a scan rate 100 mV $s^{-1}$. According to the equation of $k_{cat,H_2O}/k_{cat,D_2O} = (i_{cat,H_2O}/i_{cat,D_2O})^2$, KIE = 1.9 for **1**.

**Table S1.** Crystallographic data and processing parameters for $[Cu(N_3Py_2)](BF_4)_2$ and $[Cu(N_2Py_3)](BF_4)_2$

| Complex | $[Cu(N_3Py_2)](BF_4)_2$ | $[Cu(N_2Py_3)](BF_4)_2$ |
|---|---|---|
| Formula | $C_{19}H_{29}N_5B_2F_8Cu$ | $C_{21}H_{25}N_5B_2F_8Cu$ |
| Formula weight | 564.63 | 584.62 |
| Crystal system | Monoclinic | Monoclinic |
| Space group | *P 1 21/n 1* | *C2/c* |
| $Z$ | 8 | 4 |
| $a$ / Å | 14.2265(18) | 14.002(4) |
| $b$ / Å | 25.288(3) | 11.085(3) |
| $c$ / Å | 14.4222(19) | 15.701(4) |
| $\alpha$ / deg | 90.00 | 90.00 |
| $\beta$ / deg | 108.422(3) | 94.935(5) |
| $\gamma$ / deg | 90.00 | 90.00 |
| $V$ / Å$^3$ | 4922.7(11) | 2428.0(1) |
| $D_{calcd}$ / g m$^{-3}$ | 1.524 | 1.599 |
| $\mu$ / mm$^{-1}$ | 0.965 | 0.982 |
| Crystal size / mm | 0.21 × 0.20 × 0.19 | 0.21 × 0.20 × 0.19 |
| $\theta$ Range / deg | 1.611 / 27.708 | 2.60 / 27.64 |
| Reflns collected / Indep. | 11442 / 7451 | 2518 / 2817 |
| Parameters refined | 761 | 170 |
| $F$(000) | 2312 | 1188 |
| GOF on $F^2$ | 1.111 | 1.146 |
| Final $R_1$ ($I > 2(I)$) | 0.0856 | 0.0438 |
| Final $wR_2$ ($I > 2(I)$) | 0.1945 | 0.1306 |
| max. peak/hole / e Å$^{-3}$ | 0.922 / -0.495 | 0.623 / -0.603 |

$R_1 = \Sigma||F_o| - |F_c||/\Sigma|F_o|$, $wR_2 = [\Sigma(|F_o|^2 - |F_c|^2)^2/\Sigma(Fo_2)]^{1/2}$

**Table S2** Selected bond lengths (Å) and angles (deg) for $[Cu(N_3Py_2)](BF_4)_2$ and $[Cu(N_2Py_3)](BF_4)_2$

| $[Cu(N_3Py_2)](BF_4)_2$ | | $[Cu(N_2Py_3)](BF_4)_2$ | |
|---|---|---|---|
| Bond lengths (Å) | | Bond lengths (Å) | |
| Cu–N1 | 2.061(4) | Cu–N1 | 1.942(2) |
| Cu–N2 | 2.013(4) | Cu–N2 | 2.069(2) |
| Cu–N3 | 1.993(4) | Cu–N3 | 2.095(2) |
| Cu–N4 | 2.020(4) | Cu–N4 | 2.095(2) |
| Cu–N5 | 2.285(4) | Cu–N5 | 2.069(2) |
| Bond angles (deg) | | Bond angles (deg) | |
| N1–Cu–N2 | 85.9(6) | N1–Cu–N2 | 80.9(0) |
| N1–Cu–N3 | 164.4(2) | N1–Cu–N3 | 130.7(4) |
| N1–Cu–N4 | 94.1(4) | N1–Cu–N4 | 130.7(4) |
| N1–Cu–N5 | 84.4(8) | N1–Cu–N5 | 80.9(0) |
| N2–Cu–N3 | 82.2(0) | N2–Cu–N3 | 80.7(3) |
| N2–Cu–N4 | 165.9(0) | N2–Cu–N4 | 111.5(8) |
| N2–Cu–N5 | 113.3(2) | N2–Cu–N5 | 161.8(0) |
| N3–Cu–N4 | 94.9(0) | N3–Cu–N4 | 98.8(4) |
| N3–Cu–N5 | 109.5(0) | N3–Cu–N5 | 111.5(9) |
| N4–Cu–N5 | 80.6(9) | N4–Cu–N5 | 80.7(4) |

**Table S3** Overpotentials and observed rate constants for mononuclear copper complexes reported as WOCs in alkaline aqueous solution (pH from 10 to 14)

| Entry | Catalyst[a] | pH | $\eta$ ( half peak overpotential) (mV)[b] | $k_{cat}$ ($s^{-1}$) | Ref. |
|---|---|---|---|---|---|
| 1 | [(6,6′-2O$^{-}$-bpy)Cu($H_2O$)$_2$] | 12–14 | 510–560 | 0.4 (pH 12.4) | S6 |
| 2 | [Cu(pyalk)$_2$] | 13.3 | 607 | 0.7 | S7 |
| 3 | [(6,6′-dhbp)$_2$Cu($CH_3OH$)]$^{2+}$ | 12.6 | 516 | 0.356 | S8 |
| 4 | [(bpy)Cu(OH)$_2$] | 12.5 | 750 | 100 | S9 |
| 5 | [Cu(pimH)($H_2O$)$_2$]$^{2+}$ | 12 | 780 | 35 | S10 |
| 6 | [CuL($H_2O$)]$^{2+}$ | 12 | 680 | – | S11 |
| 7 | [(L1)Cu]$^{2-}$ | 11.5 | 700 | 3.56 | S12 |
| 8 | [(L2)Cu]$^{2-}$ | 11.5 | 400 | 3.58 | S12 |
| 9 | [(L3)Cu]$^{2-}$ | 11.5 | 270 | 0.43 | S12 |
| 10 | [(L4)Cu]$^{2-}$ | 11.5 | 170 | 0.16 | S12 |
| 11 | [(bztpen)Cu]$^{2+}$ | 11.5 | 950 | 13.1 | S13 |
| 12 | [(dbzbpen)Cu($OH_2$)]$^{2+}$ | 11.5 | 850 | 18.7 | S13 |
| 13 | [(2G$H^{2-}$)Cu($H_2O$)] | 11 | 803 | 53 | S14 |
| 14 | [(3G$^{2-}$)Cu($H_2O$)] | 11 | 771 | 24 | S14 |
| 15 | [(TG$G^{4-}$)Cu($H_2O$)]$^{2-}$ | 11 | 621 | 33 | S15 |
| 16 | [(opba)Cu]$^{2-}$ | 10.8 | 1010 | 1.13 | S16 |
| 17 | [pdca–Cu$^{II}$–$CO_3H$]$^{-}$ | 10 | 762 | 20.1 | S17 |
| 18 | [($N_3Py_2$)Cu]$^{2+}$ (**1**) | 11 | 887 | 4.97 | This work |
| 19 | [($N_2Py_3$)Cu]$^{2+}$ (**2**) | 11 | 831 | 0.83 | This work |

[a] The structures of the catalysts listed in Table S3 are given below.

[b] The half peak overpotentials of several WOCs are estimated in their CV curves.

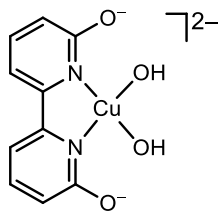

$[(6,6'\text{-}2O^{-}\text{-bpy})Cu(OH)_2]^{2-}$

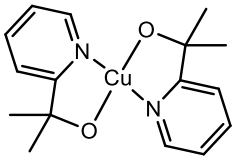

$Cu(pyalk)_2$

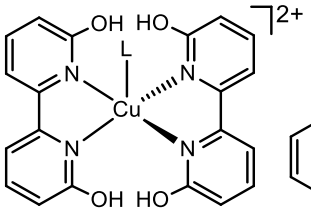

L = $CH_3OH$

$[(6,6'\text{-dhbp})_2Cu(CH_3OH)]^{2+}$

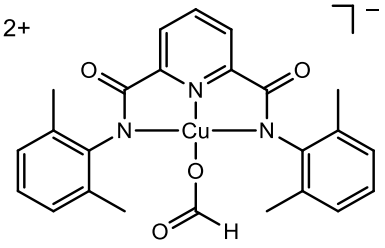

$[pdca\text{-}Cu^{II}\text{-}CO_3H]^{-}$

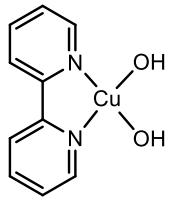

$[(bpy)Cu(OH)_2]$

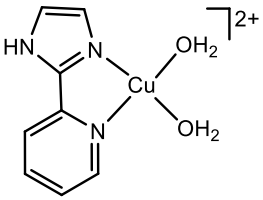

$[Cu(pimH)(H_2O)_2]^{2+}$

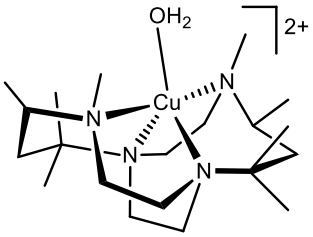

$[CuL(H_2O)]^{2+}$

L = (5*R*,12*S*)-4,5,7,7,11,12,14,14-octamethyl-1,4,8,11-tetraazabicyclo[6.6.2]hexadecane

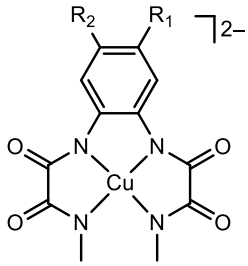

L1: $R^1 = R^2 = H$

L2: $R^1 = R^2 = Me$

L3: $R^1 = H$, $R^2 = OMe$

L4: $R^1 = R^2 = OMe$

$[(Ln)Cu]^{2-}$ (n = 1–4)

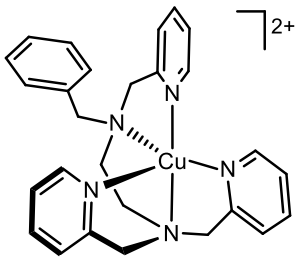

$[(bztpen)Cu]^{2+}$

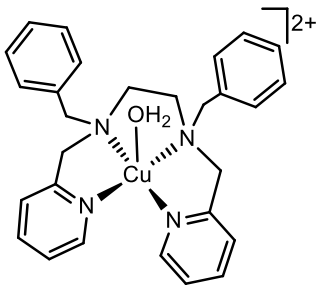

$[(dbzbpen)Cu(OH_2)]^{2+}$

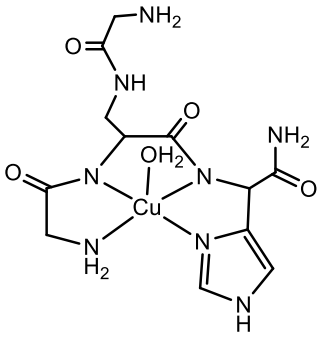

$[(2GH^{2-})Cu(H_2O)]$

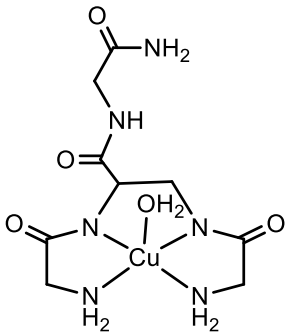

$[(3G^{2-})Cu(H_2O)]$

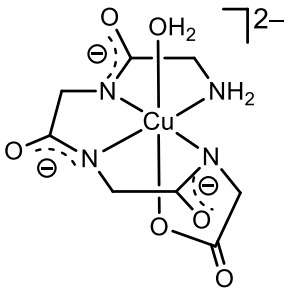

$[(TGG^{4-})Cu(H_2O)]^{2-}$

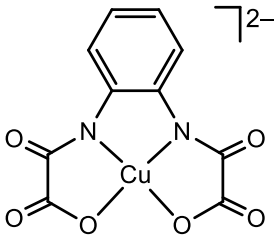

$[(opba)Cu]^{2-}$

**References**

S1 D. D. Narulkar, A. K. Srivastava, R. J. Butcher, K. M. Ansy and S. N. Dhuri, *Inorg. Chim. Acta*, 2017, **467**, 405–1414.

S2 Z. Xu, Z. Zheng, Q. Chen, J. Wang, K. Yu, X. Xia, J. Shen and Q. Zhang, *Dalton Trans.*, 2021, **50**, 10888–10895.

S3 G. M. Sheldrick, SHELXTL97 Program for the Refinement of Crystal Structure, University of Göttingen, Germany, 1997.

S4 Software packages SMART and SAINT, Siemens Energy & Automation Inc., Madison, Wisconsin, 1996.

S5 G. M. Sheldrick, SADABS Absorption Correction Program, University of Göttingen, Germany, 1996.

S6 T. Zhang, C. Wang, S. Liu, J.-L. Wang and W. Lin, *J. Am. Chem. Soc.* 2014, **136**, 273–281.

S7 K. J. Fisher, K. L. Materna, B. Q. Mercado, R. H. Crabtree and G. W. Brudvig, *ACS Catal.* 2017, **7**, 3384–3387.

S8 D. L. Gerlach, S. Bhagan, A. A. Cruce, D. B. Burks, I. Nieto, H. T. Truong, S. P. Kelley, C. J. Herbst-Gervasoni, K. L. Jernigan, M. K. Bowman, S. Pan, M. Zeller and E. T. Papish, *Inorg. Chem.* 2014, **53**, 12689–12698.

S9 S. M. Barnett, K. I. Goldberg and J. M. Mayer, *Nat. Chem.* 2012, **4**, 498–502.

S10 L. A. Stott, K. E. Prosser, E. K. Berdichevsky, C. J. Walsby and J. J. Warren, *Chem. Commun.* 2017, **53**, 651–654.

S11 J. Wang, H. Huang and T. Lu, *Chin. J. Chem.* 2017, **35**, 586–590.

S12 P. Garrido-Barros, I. Funes-Ardoiz, S. Drouet, J. Benet-Buchholz, F. Maseras and A. Llobet, *J. Am. Chem. Soc.* 2015, **137**, 6758–6761.

S13 J. Shen, M. Wang, P. Zhang, J. Jiang and L. Sun, *Chem. Commun.* 2017, **53**, 4374–4377.

S14 J. S. Pap, L. Szyrwiel, D. Sranko, Z. Kerner, B. Setner, Z. Szewczuk and W. Malinka, *Chem. Commun.* 2015, **51**, 6322–6324.

S15 M.-T. Zhang, Z. Chen, P. Kang and T. J. Meyer, *J. Am. Chem. Soc.* 2013, **135**, 2048–2051.

S16 L.-Z. Fu, T. Fang, L.-L. Zhou and S.-Z. Zhan, *RSC Adv.* 2014, **4**, 53674–53680.

S17 F. F. Chen, N. Wang, H. T. Lei, D. Y. Guo, H. F. Liu, Z. Y. Zhang, W. Zhang, W. Z. Lai and R. Cao, *Inorg. Chem.*, 2017, **56**, 13368–13375.